Manufacturing catalyst-coated membranes by ultrasonic spray deposition for PEMFC: Identification of key parameters and their impact on PEMFC performance

Zarina Turtayeva, Feina Xu, Jérôme Dillet, Kévin Mozet, Regis Peignier, Alain Celzard, Gaël Maranzana

Manufacturing catalyst-coated membranes by ultrasonic spray deposition for PEMFC: identification of key parameters and their impact on PEMFC performance

Zarina Turtayeva[1], Feina Xu[1, *], Jérôme Dillet[1], Kévin Mozet[1], Régis Peignier[2], Alain Celzard[2], Gael Maranzana[1]

1. Université de Lorraine, CNRS, LEMTA, F-54000 Nancy, France
2. Université de Lorraine, CNRS, IJL, 88000 Épinal, France

* corresponding author: feina.xu@univ-lorraine.fr
Tel: +33 372 744 253

Keywords: Pt/C catalyst powders, catalyst-coated membranes (CCMs), ultrasonic spray coating, morphological and electrochemical characterization, Proton-exchange membrane fuel cells (PEMFCs)

Abstract

This study deals with the manufacturing of catalyst-coated membrane (CCMs) for newcomers in the field of coating. Although there are many studies on electrode ink composition for improving the performance of proton-exchange membrane fuel cells (PEMFCs), there are few papers dealing with electrode coating itself. Usually, it is a know-how that often remains secret and constitutes the added value of scientific teams or the business of industrialists. In this paper, we identify and clarify the role of key parameters to improve coating quality and also to correlate coating quality with fuel cell performance via polarization curves and electrochemical active surface area measurements. We found that the coating configurations can affect the performance of lab-made CCMs in PEMFCs. After the repeatability of the performance obtained by our coating method has been proved, we show that: (i) edge effects, due to mask shadowing - cannot be neglected when the active surface area is low, (ii) a heterogeneous thickness electrode produces performance lower than a homogeneous thickness electrode, and (iii) the origin and storage of platinum on carbon powders are a very important source of variability in the obtained results.

1. Introduction

A proton-exchange membrane fuel cell (PEMFC) can be considered as a clean electrochemical energy device, since the only by-product is water. It is supplied with hydrogen at the anode side and oxygen at the cathode side to produce electricity and heat. The electrochemical conversion of the two gases is possible thanks to the presence of a membrane electrode assembly (MEA), which is composed of a proton exchange membrane, two catalyst layers, and two gas diffusion layers (GDLs). Due to its key role, MEA is called the heart of a PEMFC.

Over the past decades, many advances have been made in the field of MEA dedicated to PEMFCs, especially through new/improved materials and manufacturing processes [1–3]. Generally, perfluorosulfonic acid (PFSA) membranes and ionomers are used for this kind of application, because of their high protonic conductivity, and good chemical and mechanical stability [4, 5]. A certain variety of these proton conductors are commercially available, either with long side-chains (Nafion®, Fumion®) or short side-chains (Aquivion®, 3M®). The membranes can be made of expanded polytetrafluoroethylene (PTFE) impregnated with ionomer, which allows to improve the mechanical stability and thus to decrease the thickness. These membranes are also stabilized by the addition of antioxidants and radical scavengers that allow the decomposition of hydrogen peroxide [6]. Most of the time, the membrane is assembled to the electrodes by hot pressing or it constitutes the support of the electrodes when the latter are deposited directly on it. However, it is possible to perform a direct membrane deposition by spraying a Nafion® ionomer onto gas diffusion electrodes (GDEs) via inkjet printing [7, 8].

Regarding the GDL, it is made of carbon-based materials and plays several roles such as mass (gas and water), heat and electron transport. As the GDL plays a key role in water management, many carbon-based materials such as carbon paper, fiber, felt or cloth have been tested and modified to tune their wettability and/or porous structure [9, 10]. The addition of a microporous layer (MPL) on top of the GDL allows to modify the hydrophobicity with respect to the electrode [11]. The obtained GDL is called GDL with MPL [12]. The general ink recipe for MPL is composed of carbon, PTFE, and solvent, but the proportion of each compound depends on the experimenters. For instance, one of the studies found that 20 wt % PTFE in the MPL gives the highest performance in PEMFC with H_2 / air at 75 °C [9], but this result is related to their operating conditions and their ink. As the researchers do not have the same experimental protocol and conditions, there are a myriad of commercial GDLs with or without

treatment and with or without MPL allowing to adapt to used materials and operating conditions [9, 11].

As far as the electrode or catalyst layer is concerned, two trends are emerging, one leading to a decrease in the amount of platinum down to an ultralow Pt loading, the other one leading to new or Pt-free catalysts. In fact, there is not enough Pt (i.e. amount and availability) in the world to meet the global demand with the Pt loading currently used in commercial fuel cell electric vehicles (FCEVs) [13–16]. Consequently, Pt must be used efficiently and/or replaced by cheaper and more abundant catalysts. All types of catalysts (based on carbon, metal or mixed) can be electrochemically characterized using a rotating disk electrode (RDE) and/or a rotating ring disk electrode (RRDE) for a first screening of their performance [17, 18]. But these methods are not sufficient to guarantee good performance in fuel cells. Indeed, a liquid electrolyte is used as a transport medium in RDE/RRDE cells. Under these conditions, the measured current is very quickly limited by the oxygen transport in the study of the oxygen reduction reaction. As a consequence, limited by mass transport, only very low current densities ($mA.cm^{-2}$) can be measured by RDE [19]. To overcome this issue, the floating electrode technique was developed to measure the data at a higher current density. Zalitis et al. [20] compared the RDE and floating electrode techniques in 4M $HClO_4$ solution in the study of the oxygen reduction reaction by Pt/C (60 wt %). While the RDE technique shows a limiting current at 14 $mA.cm^{-2}$, the floating electrode technique can operate up to 180 $mA.cm^{-2}$. Although there is an improvement in the range of measured currents, it is still far from the current range of PEMFCs, rationalizing here the need for testing active layers in single fuel cells.

To ensure proper catalyst behavior or optimal Pt loading in the fuel cell environment, the inks must be prepared and deposited on an appropriate support. The catalyst can be deposited directly on the membrane or on the GDL, resulting two types of MEAs: a catalyst-coated membrane (CCM), known as CCM-based MEAs or a gas diffusion electrode (GDE), referred to as GDE-based MEAs. In addition, some authors used the transfer decal method to prepare a CCM by indirect deposition [1, 21–23]. They deposited the catalyst on an inert support such as fluorinated ethylene propylene, a virgin electrical grade film of PTFE or aluminum foil, and then transferred the deposited layer onto a membrane [1, 21]. When the coating is performed on an inert support, the difficulty remains to properly transfer the deposited layer from the inert support to the membrane via hot pressing. But when a coating technique and the use of different supports are mastered, MEAs prepared with different supports can give comparable PEMFC performance. Indeed, Shahgaldi et al. [1] compared different methods of fabricating MEAs using GDL, membrane, and an inert substrate with a commercial

spray gun with nitrogen as a pressurized stream. At a Pt loading of 0.5 mg.cm^{-2}, the optimized MEAs with the three supports gave a similar power density near 0.90 W.cm^{-2} (PEMFC at 75 °C with fully humidified H_2 and air), although that of the CCM-based MEA without hot pressing was slightly higher (near 0.93 W.cm^{-2}) than the other two supports. The results of this work suggest that support is not a key point, but that the way of coating and also the formulation of the ink, depending on the coating method and the support, matter in the performance of the PEMFC.

Nowadays, there are a large number of commercial coating methods for the manufacturing of MEAs based on different materials, such as screen and inkjet printing methods, doctor blade coating method, gravure method, roll-to-roll method, slot-die method, spray-, electrospray-, gun spray-, and ultrasonic spray-coating devices [7, 8, 32–37, 24–31]. Depending on the properties of the ink, the amount of catalyst powder or the support chosen, one coating method can be favored over another one. For instance, a roll-to-roll method may not be suitable at the laboratory scale for testing new catalysts, which are produced in a small amount (a few milligrams). Concerning the support, it appears to us that the electrospray technique is more suitable to GDL than to membrane, because this technique must impose a voltage drop of about 9 kV between the nozzle head (needle) and the collecting substrate.

In this paper, we have chosen to focus on the ultrasonic spray coating method with the perspective to test new carbon-based catalysts in the near future. This technique can be used to prepare samples on a laboratory scale and appears to be suitable for all types of support. According to the literature, samples prepared by ultrasonic spray coating can possess good porosity, homogeneity, and distribution of nanoparticles on the surface of the deposited layer [27, 30, 38–41]. Martin et al. [38] compared the surface microstructure of the different catalytic layers (CL) obtained with different catalyst coating methods such as ultrasonic spray, air brushing, and electrospray for a given ink composition. The authors showed that the GDE obtained by ultrasonic spray coating exhibited the smoothest surface dotted with several Pt / C aggregates of about 50-80 µm in size. The least uniform surface was obtained by the air brushing technique due to the absence of ultrasonic generator in the nozzle head, which deagglomerates particles prior to coating. However, the study of porosity pointed out that the GDE prepared by electrospraying had higher porosity than the sample prepared by ultrasonic spraying (70 vs. 49 %, respectively). Besides, Sassin et al. [39] recently showed that the pore size distribution remains unchanged, but the porosity decreases with the increase of catalytic layer thickness fabricated by ultrasonic spray.

Although the decrease in porosity of the catalytic layer obtained with the ultrasonic spray coating method may alter gas and water transport in an operating PEMFC, this coating method can be interesting for studying new catalysts based on metal-free carbon. In fact, the latter may agglomerate rapidly in an ink dispersion and it could be difficult to disperse them homogeneously without the help of the ultrasonic generator in the head of the nozzle. Indeed, this feature can provide a more uniform range of particles dispersed on a substrate. Although this function is quite convenient for dealing with certain dispersions with agglomeration issues, some know-hows is still needed to grasp and learn the proper use of ultrasonic spray-coating. To do this, an ink has to be prepared before setting the operating parameters of the coating machine. But it is quite confusing for newcomers to see that a myriad of ink compositions are available in the literature and often one does not know what criteria to choose them. Indeed, the ink can be prepared with: (i) different solvents such as water, ethanol or isopropanol, (ii) different Nafion® ionomer contents, varying typically between 5 to 20 wt %, and (iii) different Pt/C by weight such as 20, 40 or 50 wt % Pt [28, 29, 32, 39]. It could be that the property of the obtained ink or the type/size of nozzle has an impact on the ink flow rate, since the latter varies according to the authors from $\mu L.min^{-1}$ to $mL.min^{-1}$. Some authors [28, 29] prepared samples with similar Pt loading, but the results cannot be objectively compared because the fuel cell tests conditions were different. Other authors used a similar spray pattern [28, 32], but the Pt loading of their samples was different. As Pt loading is proportional to the number of coating layers and also to the amount of Pt/C in the ink, it can have an impact on the thickness of the catalyst layer, as well as on the performance of PEMFC [29, 39]. Moreover, the thicker the catalyst layer, the lower the total pore volume of the coatings [38], which can hinder mass transport. In addition, the topology of the coatings can change depending on the spray pattern. Deschamps et al. [42] tested two spraying configurations with and without spacing at the nozzle return and showed that the topology of the obtained deposited layers varies with the spraying configurations, suggesting a possible variation in PEMFC performance.

From the data reported in the literature, it seems to us that a reproducible and repeatable coating is not as easy to obtain as may seem at first sight. The ink formulation and coating step are of great importance in evaluating the catalyst layer as well as new catalysts [28, 29, 32, 39, 43–45]. This step is very difficult to rationalize because of the many parameters involved, such as the surface properties of the materials, their interaction with solvents, with any additives used to adjust porosity or viscosity, ink mixing and stabilization methods, and coating parameters. In the case of spray coating, these include nozzle speed, nozzle height, nozzle size or type, ink flow rate, substrate temperature, ink homogenization technique, MEA post-treatment, etc. In

the end, the optimal process to manufacture MEA is rather a know-how that often remains secret and constitutes the added value of scientific teams or the business of industrialists. Evaluation of new materials in a rigorous and reproducible way requires the learning of this know-how, which is why it is important from our point of view to communicate on this subject.

Although a lot of information is shared in the literature on how to coat with an ultrasonic spray coating machine [28, 29, 31, 32, 38], there are still some other aspects to pay attention to when starting in the field of coating, especially spray configurations and patterns, the mask and preservation of the Pt/C powder. Thus, this work attempts to link some coating parameters with coating modeling coupled with the performance of the CCMs obtained during PEMFC tests, such as polarization curves and physicochemical characterizations. We would like among others to check whether it is possible to predict the shape of the coating via simulation. This can be used to optimize the pitch (index space distance) between two lines as a function of the thickness profile for one layer. The comparison of simulated and measured thicknesses can also give information on the penetration of the upper layers into the lower layers, which is a source of porosity reduction. Ultimately, we would like to save beginners in the field of coating from having unsuccessful experiences and to be able to gain time in the early stages of coating, as effective coating of CCMs becomes more and more important in research laboratories due to the booming fuel cell markets and projects worldwide.

2. Experimental part

2.1. Materials

Alcohol based 1100 EW at 20 wt % Nafion dispersion (D2021) and 40 wt % Pt/C powders named FCS 40 % Pt/C-Vulcan XC-72R (2019) and FCS 40 % Pt/C-Black (2020) were purchased from Fuel Cell Store. 40 wt % Pt/C powders called AA 40 % Pt/C (2020) and AA 40 % Pt/C (2021) were also purchased from Alfa Aesar for comparison. Here, the numbers in brackets after the called name of the catalysts refer to the year of purchase. 99.8 % isopropanol was purchased from Carlo Erba. Nafion®212 membranes were purchased from Ion Power. Sigracet® GDLs 28BC with a microporous layer and PTFE (5 wt %) were purchased from Fuel Cell Store.

High-purity water (18 MΩ) was used in this work. All coating layers were obtained with an automatic ultrasonic spray bench (ExactaCoat) from SonoTek. An ACCUMIST nozzle (120 kHz) was used in this work. A 10 mm-thick glass mask and a 1 mm-thick polycarbonate (PC) mask were used during coating.

A Dektak XT tactile profilometer (Bruker) was used to measure the thickness of the deposited layers. The probe size of the profilometer was 2 µm and the measurement error was about 10 nm. The measurement step varied depending on the time required to perform the measurement. The maximum sample length that the device could measure was 4 cm.

2.2. Preparation of CCMs using an ultrasonic spray bench

2.2.1. Preparation of the catalyst ink

The general recipe for the ink preparation remained the same regardless of the Pt/C powder supplier. The ink was composed of 0.4 g of Pt/C in a 1:2 mixture of water and isopropanol. The ratio of Nafion® ionomer (*R*(*Nafion ionomer*)) in the dispersion was 0.33 and it is expressed according to Equation (1).

$$R(Nafion\ ionomer) = \frac{m(Nafion(solid)\ ionomer)}{m(Nafion(solid)\ ionomer) + m(catalyst\ powder)} \quad (1)$$

where $m(Nafion(solid)\ ionomer)$ is the mass of Nafion ionomer in solid form and $m(catalyst\ powder)$ is the mass of catalyst powder in the dispersion.

Each ink was prepared in 100 mL vial with a screw cap in order to prevent evaporation of the isopropanol. A stirring bar was used to mix the dispersion. The first step was to introduce the desired amount of Pt/C powder and water to avoid ignition of Pt upon encountering isopropanol. Then, isopropanol and Nafion® ionomer were poured inside the vial. At each intermediate step, an ultrasonic bath was used for at least 1 h to spread the particles in the dispersion. In addition, the final step of the ink preparation was obtained after one night in ultrasonic bath (Elmasonic S10, 37 kHz, 30 W). The prepared ink was used within 3 days to prevent ink settling and evaporation of solvent. When the prepared ink was not used for coating, it was placed under magnetic stirring. Before reuse, the prepared and stirred ink was introduced into an ultrasonic bath for at least 1 hour. Once the suspension was ready, an amount of ink was pumped into the syringe of the coating machine.

2.2.2. Calculation of the Pt loading

As is well known, Nafion® membrane has the particularity to swell in the presence of humidity or hydrophilic solvents. Due to this behavior, the mass of the membrane is not stable

when weighed carelessly at a given temperature. During spray coating, the temperature used affects the hydration of the pristine Nafion® and therefore its mass as well. For this reason, we had to resort to the use of a piece of aluminum foil to estimate the Pt loading during coating. Calculation of the Pt loading (L_{Pt}) is obtained by equations (3) to (6).

$$R(Catalyst\ powder) = 1 - R(Nafion\ ionomer) \quad (3)$$

$$m_{deposited} = m_f - m_i \quad (4)$$

where $R(Catalyst\ powder)$ is the ratio of catalyst powder in the dispersion, m_f is the mass at the end of the coating of the piece of aluminum foil and m_i is the mass of the pristine piece of aluminum foil.

$$m_{Pt} = m_{deposited} \times R(Catalyst\ powder) \times R(Pt\ wt) \quad (5)$$

where $R(Pt\ wt)$ is the ratio of Pt in the catalyst powder. For instance, it is 0.4 for Pt at 40 wt %.

$$L_{Pt} = \frac{m_{Pt}}{S_A} \quad (6)$$

where S_A is the active surface area (7.22 cm^2 in our work). Of course, the estimation of L_{Pt} is only valid if we assume that the ink dispersion is homogeneous during the spray-coating steps.

2.2.3. Coating program and its modeling

The spray bench is composed of a mobile spraying nozzle in 3 dimensions (*x*, *y* and *z*) and a heating plate on which the coating support is placed. The spraying suspension is connected to a 25 mL syringe through connecting tubes. Due to the mobility of the nozzle head, the length of the connecting tubes cannot be neglected. Therefore, a dead volume of about 10 mL must therefore be taken into account when preparing the catalyst ink. The flow rate of the catalyst ink, the speed of the spray nozzle and its trajectory can be adjusted via the bench software. Before setting these parameters, we must first determine the nozzle stall point for each ink. The stall point can be defined as the limit power (in Watts (W)) where atomization ends or begins. As the properties of the formulated inks differ from one to another, the value of the stall point obviously cannot be the same. In our study, the stall point for both inks was close

to 1.5 W. Then, the flow rate and nozzle velocity were fixed at 0.1 mL.min^{-1} and 5 mm.s^{-1}, respectively. The temperature of the heating plate was set at 90 °C. A serpentine pattern was chosen for the spray coating. Following the work of Sassins et al. [46], a similar approach was applied throughout this work. To ensure a rather homogeneous coating, 2 vertical and 2 horizontal serpentine paths were used to cover the blank interline of each serpentine pattern. Due to the curvature of the serpentine pattern when the direction of the spray is changed, the edges of the coating area were heterogeneous as depicted in Fig. 1. Therefore, the use of a mask is crucial to achieve a well-defined edge.

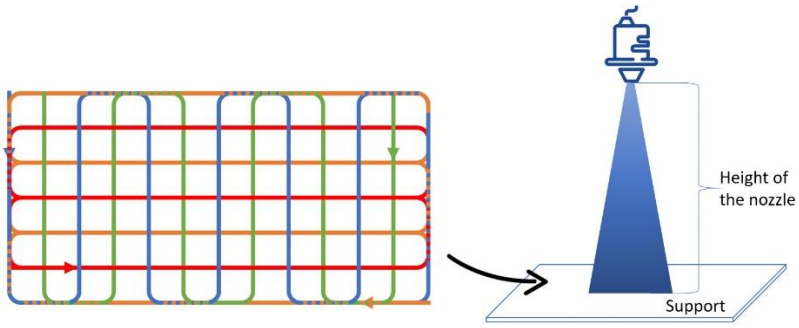

Figure 1. Scheme of the spray pattern shape according to the height of the nozzle (1st run path in blue (vertical), 2nd run path in orange (horizontal), 3rd run path in green (vertical) and 4th run path in red (horizontal)).

The nozzle used creates a cone-shaped spray as shown in Fig. 1. Depending on the height of the nozzle, the deposited line does not have the same total width on the support or the same width of homogeneous part of the catalyst layer (Figs. 2(a) and 2(b)). The deposited line appears well defined when the support is close to the nozzle head (within 20 mm). However, some supports can be deformed by solvents or the deposited particles can be detached from the support because of the spray force when the nozzle is too close to the support.

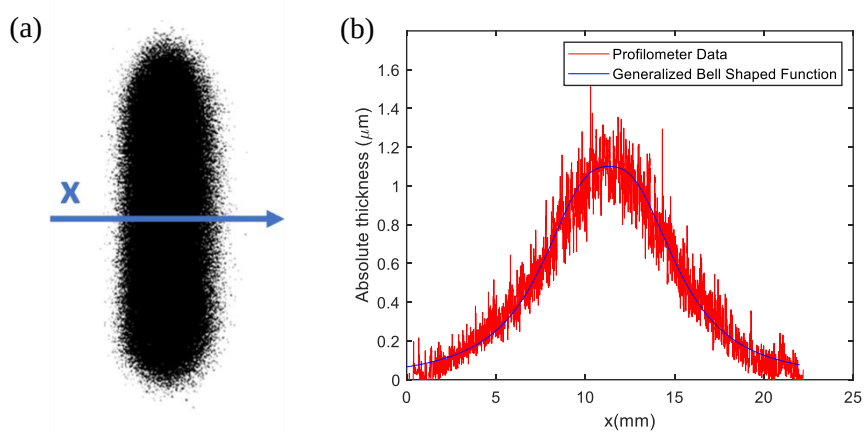

Figure 2. (a) 4 spray lines of the catalyst ink prepared with AA 40 % Pt/C (2021) under a nozzle height of 60 mm; (b) profile thickness measured according to x by the profilometer and generalized bell-shaped function fit (GBSF) f(x;4,1.3,11.3,1.1µm) obtained MatLAB [Maximum thickness of 4 layers ≈ 4.4 µm].

To model the coating configuration and pathway, first we have to fit one spray line of the coating layer. Thus, a sample was prepared on a glass support at the nozzle height of 60 mm and the thickness profile of the obtained sample was measured by a tactile profilometer. The profilometer data shown in Fig. 2 (b, red line) is obtained by accumulating 4 spray lines. Here, we assumed that the quality of each spray line is equivalent to one other. Because the measured data is well matched, a generalized bell-shaped membership function (GBSF), in equation (7), is chosen to fit the profilometer measurement in MatLAB using the least-squares fitting method (Fig. 2 (b, blue line).

$$f(x;a,b,c,A_L) = \frac{1}{1+\left|\frac{x-c}{a}\right|^{2b}} \times A_{1L} \tag{7}$$

The generalized bell-shaped membership function is symmetric. As expressed in equation (7), this function uses four parameters: a determines the width of the bell-shaped curve, b is a positive integer, c defines the center of the curve [47], and A_{1L} is the amplitude of a spray layer, that is the total thickness divided by 4 (Fig.2(b)).

Besides, the index space was chosen to be 50 % of the maximum intensity of the generalized bell-shaped function, which corresponds to 0.7 cm in our case.

A mask was used to avoid the inhomogeneity of the spray on the 4 edges. Since the use of a mask leads us to coat a larger area, the actual sprayed area was set at 4.2 × 2.1 cm^2

considering the value of the index space (0.7 cm here). In order to achieve the desired active area of 3.8 × 1.9 cm^2, the first and third run paths (blue and green lines in Fig. 1, respectively) were composed of 6 and 5 vertical serpentine lines spaced 3.5 mm apart, respectively. The second and fourth run paths (orange and red lines in Fig. 1, respectively) were composed of 3 and 2 horizontal serpentine lines spaced 3.5 mm apart, respectively. Furthermore, the coating simulation was defined for the desired active area and is discussed in Section 3.

2.3. Electrochemical characterization in a working fuel cell bench.

The prepared CCMs were tested on a lab-made fuel cell test bench to evaluate their performance via polarization curves and electrochemical surface area (ECSA) measurements. The fuel cell was mounted in counterflow mode with two 28BC GDLs and two PTFE gaskets (150 µm).

Prior to any fuel cell bench testing, a conditioning step is needed to ensure membrane hydration and catalyst activation. The conditioning was performed as literature [48, 49]. This step consists of cycling the voltage between OCV (Open Circuit Voltage), 0.3 V and 0.6 V every 30s for at least 6h. The operating conditions were 70 °C and 60 % relative humidity for air and hydrogen. During this step, the flow rates were calculated according to the previously measured currents and at an air H_2 / air stoichiometry of 1.5/4. After this step, electrochemical characterizations were performed, such as: (i) polarization curves, which represent the performance of the fuel cell in given operating conditions, (ii) cyclic voltammetry, to evaluate the ECSA of the catalyst. All these characterizations were carried out automatically using lab-made LabVIEW programs. Each time, two configurations described in Fig. 3 were used to test the homogeneity of the prepared CCM. It was assumed that if the both sides of a prepared CCM are similar, then they should give a similar performance in PEMFC regardless the configuration of the cell. Therefore, the two configurations of the cell performance were tested and the performance in PEMFC was compared via polarization curves.

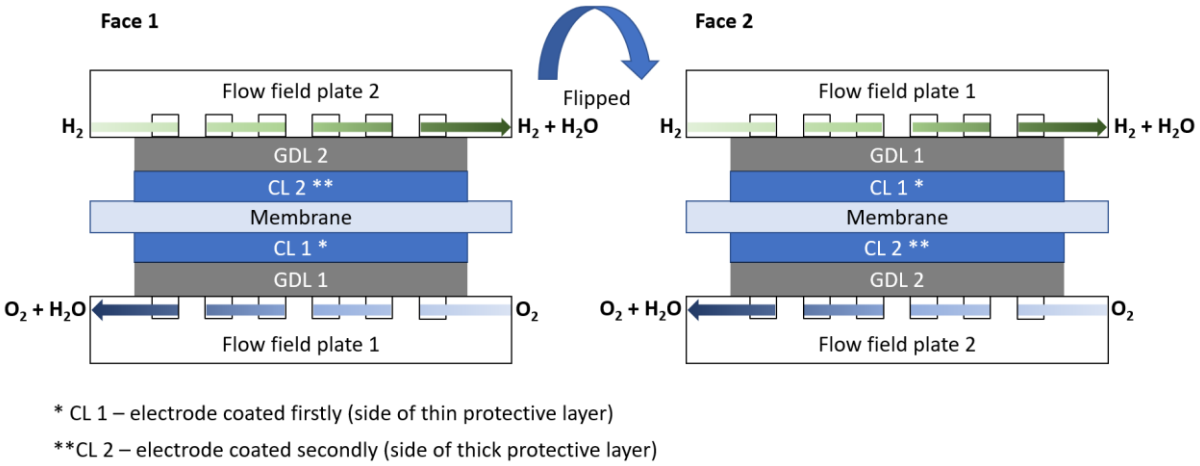

* CL 1 – electrode coated firstly (side of thin protective layer)

**CL 2 – electrode coated secondly (side of thick protective layer)

Figure 3. Face 1 and Face 2 configurations, where the anode side is at the top and the cathode side at the bottom of each configuration.

2.3.1. Polarization curves

After the conditioning step, polarization curves were performed with air and H_2 stoichiometry of 5 and 1.5, respectively. The other working conditions remained the same as for the conditioning step. Each polarization curve resulted in an average of two measurements of voltage versus current. The first measurement started at 0 A (OCV) and the current was gradually increased until the measured voltage reached 0.3 V. The second measurement started at the last point of the first measurement. The current was progressively decreased until it reached 0 A. Each current step took 60 s and the average of the measured voltage was calculated.

2.3.2. Cyclic voltammetry

Cyclic voltammetry tests were performed to evaluate the ECSA of the prepared CCMs. The fuel cell was operated in the H_2 / N_2 mode (anode and cathode, respectively). The voltage sweep rate was 50 $mV.s^{-1}$ and the voltage range was between 0.1-0.7 V (Fig 4(a). The operating flow rates, temperature, and relative humidity of the two gases were set at 70 °C and 60 %, respectively. Cyclic voltammetry measurements were repeated at least three times for each sample. Then, the mean hydrogen adsorption/desorption charge, Q_H was analyzed in Eq. (8), was determined by integrating the two hydrogen adsorption/desorption peaks across the obtained cyclic voltammetry curves.

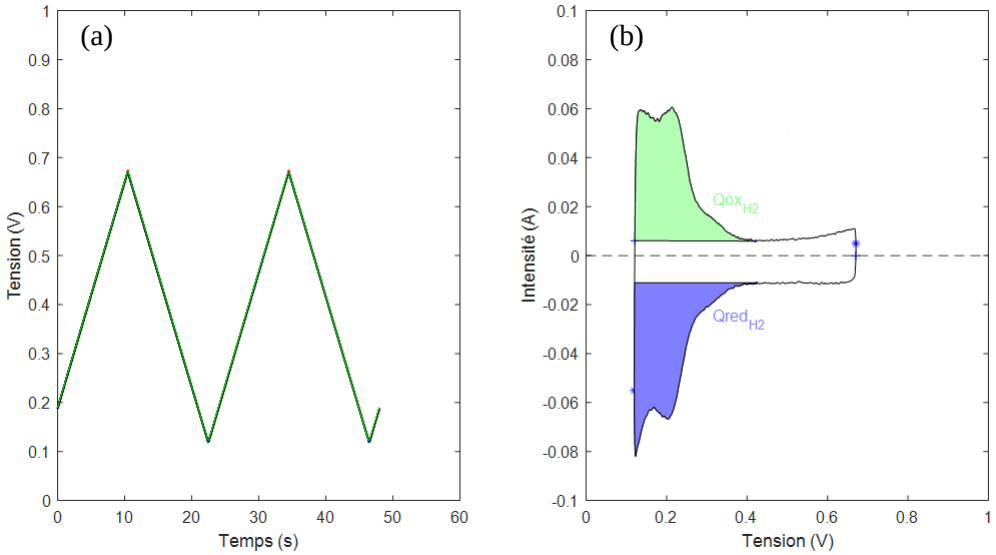

Figure 4. Cyclic voltammogram illustrating the evaluation of the ECSA: FCS 40 % Pt/C-Vulcan (2019) 0.34 $mg_{Pt}.cm^{-2}$ in the nitrogen flow humidified to 60 % RH, recorded at a sweep rate of 50 $mV.s^{-1}$

Subsequently, the ECSA was calculated by Equation (9).

$$Q_H = \frac{(Q_{ox} - Q_{red})}{2} \tag{8}$$

$$ECSA = \frac{Q_H}{210\,\frac{\mu C}{cm_{pt}^2}.L_{pt}} = \left[\frac{m^2}{g_{pt}}\right] \tag{9}$$

where, 210 $\mu C.cm^{-2}_{Pt}$ is the value of the platinum charge density when monolayer adsorption of hydrogen on the surface of platinum crystallites is assumed.

3. Results and discussion

3.1. First characterizations of the deposited electrode

3.1.1. Estimation of the Pt loading

The Pt mass loading is important to evaluate the stability of the ink over the coating time. For this purpose, a series of deposited masses (not shown) on an aluminum foil was carried out as support by applying the coating program at 60 mm from the nozzle height. During two hours of coating, each cycle (4 serpentine layers) of spray coating resulted in an average of 0.11±0.01 $mg.cm^{-2}$ of Pt loading (thus 3 cycles were necessary to reach about 0.3 $mg.cm^{-2}$ of Pt loading). However, a fluctuation in the deposited masses (> 0.01 $mg.cm^{-2}$) was observed

after this time. This fact can be explained by the local aggregation of particles in the tube over time. To avoid this problem as much as possible, the coating step lasted less than 2h. The unused ink was removed from the tube and re-mixed in its vial with a sonication step for at least 1h. Due to the mixing of the ink, a new estimation of the Pt loading (at least 2 samples) was performed after filling the tube of the ultrasonic spray coater.

3.1.2. Simulation according to the run path

Here, we attempted to evaluate the amount of particles deposited along the studied axis when depositing 1, 2, 3 or 4 spray layers in the defined area using the MatLAB software. We assumed that a homogeneous layer gives a homogeneous distribution along the studied axis. Since the GBSF fit function of one spray line is known for a given ink, we suppose that each coated layer is composed of a sum of several single spray lines separated by the index space distance. For instance, the first coating layer is composed of n single spray lines in the vertical direction, according to the width of the desired spray area. The second coating layer is composed of m singles spray lines in the horizontal direction, according to the length of the wished spray area. The third and fourth coating layers are the repetitions of the first and second layers, respectively, but shifted by the index space. In order to compare the profile thickness for each coating layer accumulation, the thickness shown in Fig. 5 is normalized for this purpose.

Fig. 5 shows the simulation of each additional layer in 3D and its top view with a mask (black rectangle), as well as a piece of profile over the length of a sample (red rectangle). Fig. 5 (1) represents the simulation of the first layer in the vertical direction. Figs. 5 (2) to (4) represent, respectively, each accumulation of layer as described above. According to our MatLAB program, each accumulation of layers decreased the empty space between each deposited line. As the simulation of the 4 layers of coating gave us the best homogeneity, we considered that a cycle of 4 serpentine pathways (as described in Fig.1) gave us a homogeneous coating. For this reason, the total number of coating layers of the prepared samples was always a multiple of the 4 layers, which is considered to be a cycle.

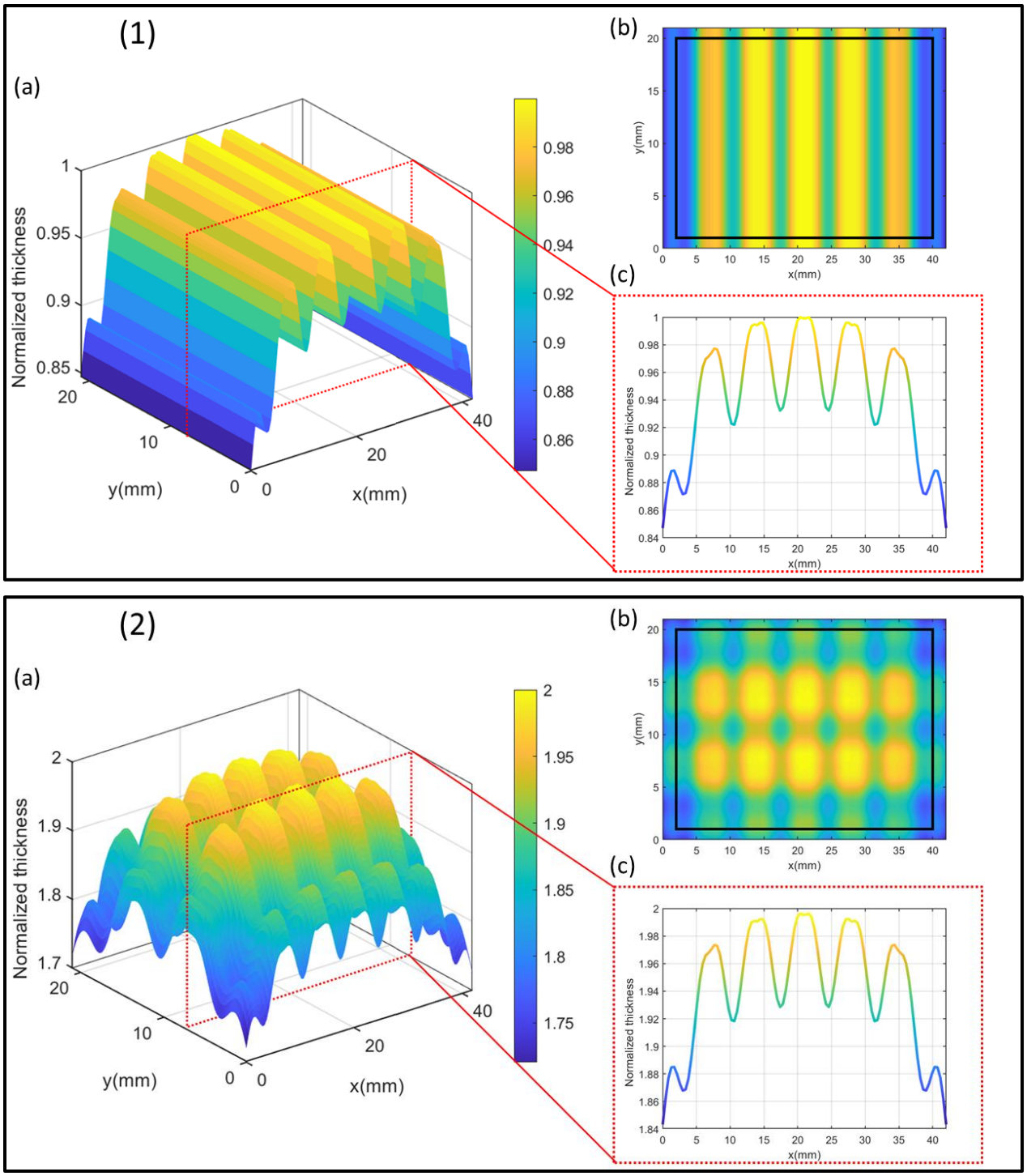
(1)
(a)
Normalized thickness
y(mm)
x(mm)
(b)
y(mm)
x(mm)
(c)
Normalized thickness
x(mm)
(2)
(a)
Normalized thickness
y(mm)
x(mm)
(b)
y(mm)
x(mm)
(c)
Normalized thickness
x(mm)

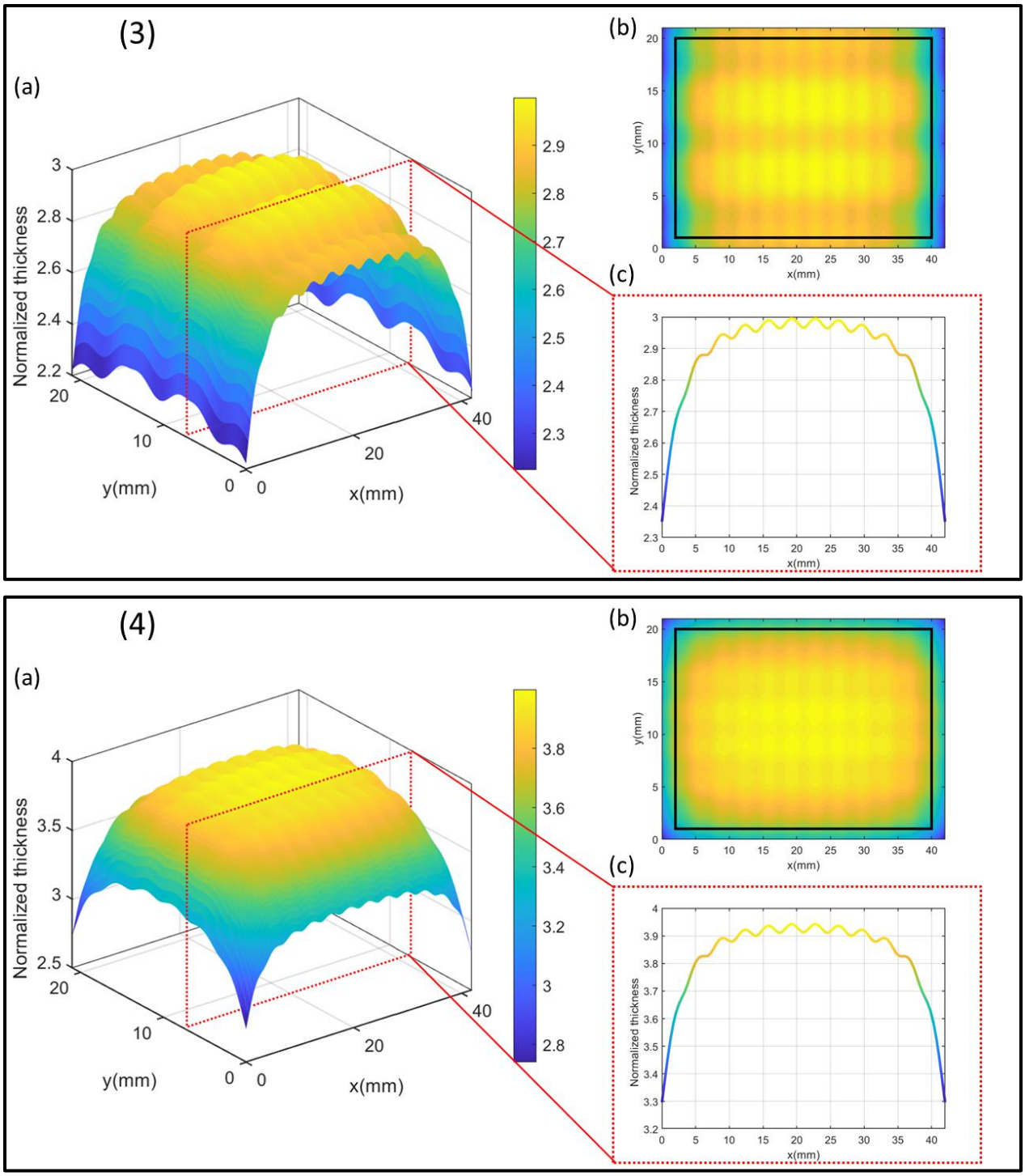

Figure 5. Contour modeling: (a) in 3D, (b) top view, and (c) profile piece along the length of the different spray layers with (1) 1 vertical serpentine layer (1st run path), (2) 1 vertical and 1 horizontal serpentine layers (1st and 2nd paths), (3) 2 vertical and 1 horizontal serpentine layers (1st, 2nd and 3rd paths), and (4) 2 vertical and 2 horizontal serpentine layers (all 4 paths).

In order to check whether our simulation can match with the measured profile thickness, samples were prepared, studied, and discussed in the forthcoming section.

3.2. Coating thickness according to masks and configurations

3.2.1. Effects of masks

Since the thickness of the coating was measured by a tactile profilometer, we had to resort to using glass as a support. Therefore, singular samples were prepared for this purpose with the constraint that the length of the samples could not exceed 4 cm. For this reason, the active surface area was divided into small portions in order to measure the thickness correctly. Here, two mask thicknesses were compared: 10 and 1 mm. The masks were made of glass and polycarbonate, respectively. The surface area ($S = 1.9 \times 3.8$ cm^2) was divided using Kapton® scotch tape, which was then removed after coating. Fig. 6 shows the different sample models prepared using different masks and obtained with 3 coating cycles at 60 mm from the nozzle height. The choice of glass mask was initially made considering that this kind of material is dimensionally stable to heat, unlike some organic polymers such as polyethylene terephthalate (PET). Since the tactile probe was 2 µm wide, it took time to do a 3D mapping. To quickly check the homogeneity of our coating surface, we measured the thickness along several guided lines drawn with different colors in Fig. 6.

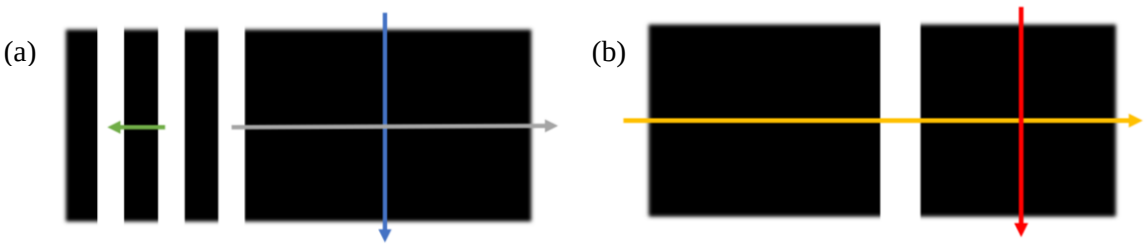

Figure 6. Samples for tactile profilometer measurements and guided lines used during measurements: (a) first sample model with glass mask, and (b) last sample model with PC mask.

The thickness of each guided line is illustrated in Fig. 7. Concerning the sample obtained with the glass mask (Fig. 7(a), 7(b) and 7(c)), we could observe that: (i) the thickness of the coating was about 11±1 µm, (ii) the measured thickness in both directions seemed to have 2 µm difference, and (iii) the coating was not homogeneous on the edges. The measured thickness was higher than that reported by Sassin et al. [39, 46] for a similar nozzle height and Pt loading. Indeed, these authors were measured by SEM 8 µm for the thickness of the catalyst layer. This

difference can be explained simply by the choice of the Pt weight fraction in the Pt/C powder, which was at 50 wt % of Pt in their work (vs. 40 wt % here). It might also be that the compression during fuel cell fabrication reduced the thickness of the catalytic layer. In addition, point (ii) above may be explained by a difference in the starting point (zero point as a reference) when changing the direction of the measurement. In fact, the size of the glass support used was 7.5 cm long and 2.5 cm wide. After coating, there was a maximum of 3 mm on each side in the width to make the zero. Even with the use of a mask, some particles might affect the measurement. The other issue is the heterogeneity of the coating. According to the modeling results in Fig. 5, there are some small heterogeneities on the surface of the coating. A difference of a few millimeters can affect the measurements of the thickness, even in one direction. Point (iii) above can be explained as follows. Contrary to the edge where Kapton® scotch tape was used, the edge where the glass mask was applied showed an amount gradient of 3 mm. This fact reveals that the thickness of the mask affects the quality of the spray on the edge of the coating as a result of a shadowing effect. By decreasing the mask thickness to 1 mm, we could decrease the amount gradient as illustrated in Fig. 7(d). Thus, the coating quality was improved by using a thinner mask to avoid the amount gradient at the edges.

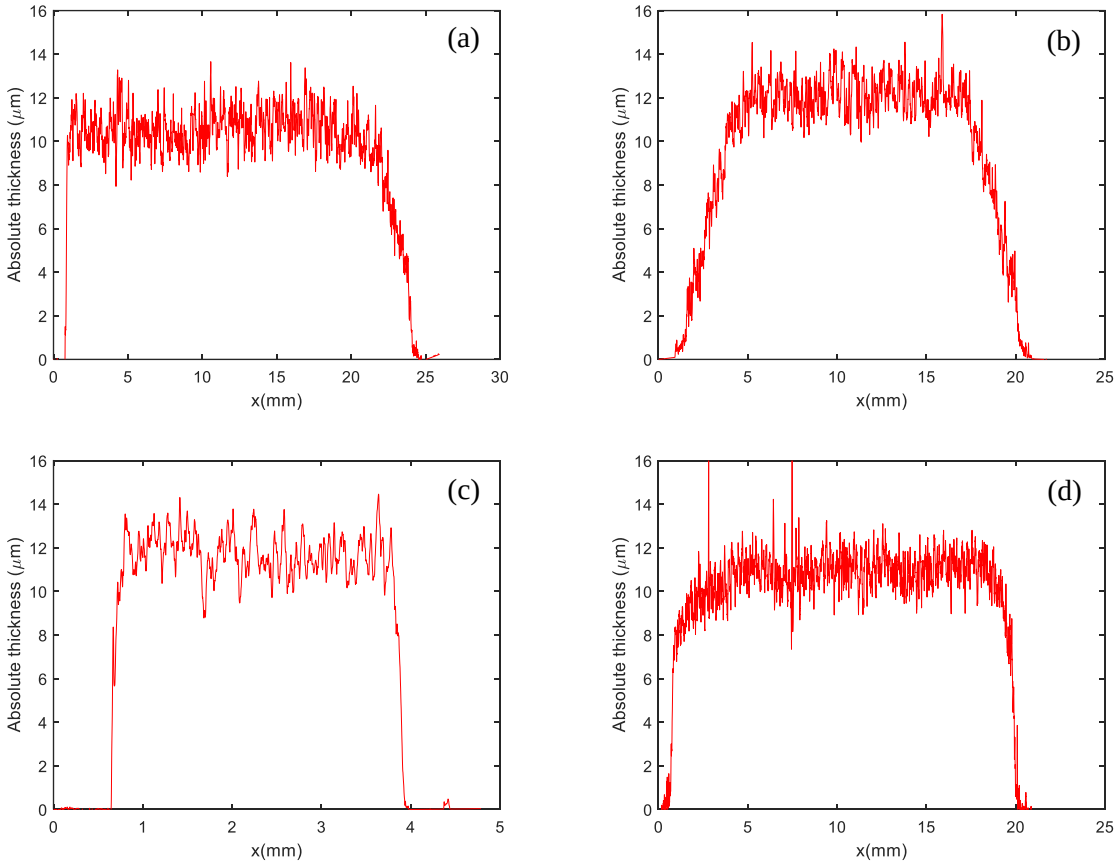

Figure 7. Profiles of deposited electrode along different guided lines: (a) gray, (b) blue, and (c) green lines in Fig. 6(a) sprayed with FCS 40 % Pt/C-Vulcan (2019) using a glass mask, and (d) red line in Fig. 6(b) sprayed with AA 40 % Pt/C (2020) using a PC mask.

3.2.2. Spray configurations

In this section, we studied the effect of spray configurations on the coating quality while keeping the PC mask. For each configuration, we attempted to fit the measured data with our MatLAB simulation program. For this purpose, three different spray configurations were chosen, namely, A – 1 vertical serpentine layer of spray pattern repeated 12 times at a nozzle height of 60 mm, B – 2 vertical and 2 horizontal serpentine layers spray pattern repeated 3 times at 40 mm from the nozzle height, and C – 2 vertical and 2 horizontal serpentine layers spray pattern repeated 3 times at 60 mm from the nozzle height. Moreover, we wanted to check whether Pt/C powders at a given Pt weight can have an impact on the coating quality. To this end, 2 Pt/C powders with carbon black as support were chosen from 2 different suppliers for this study: FCS 40 % Pt/C-black (2020) and AA 40 % Pt/C (2021). Therefore, a total of six samples were prepared as shown in Fig. 6(b), and a piece of their thickness profile was plotted along the yellow line. Fig. 8 shows the measured thickness profile of the two different catalysts sprayed in the three different spray configurations (A, B, and C). As expected, the shape of the coating depended greatly on the choice of coating configurations regardless of the Pt/C powders chosen. A in Fig. 8(a) gives us the greatest variation and heterogeneity of the coating surface. This result was expected because one path was repeated 12 times and it is comparable to the simulated result using MatLAB software with GBSF (Generalized Bell-shaped Function in Fig. 8(a) blue line). Additionally, the difference in homogeneity across configurations is consistent with the results obtained by Deschamps et al. [42], who compared the topography of sprayed layers obtained with 2 configurations of run paths and with an accumulation of 160 run paths at 33 mm height. It should be noted that the authors needed a large accumulation of layers to reach an average thickness of 6.3 µm with the commercial carbon XC-72R from Cabot®. This fact highlights the difference in ink formulation and composition between the experimenters. Concerning now the samples prepared with the configure B and C (i.e. ink deposited following 2 vertical and 2 horizontal serpentine layers repeated 3 times, but at different height of nozzle), the measured thickness profiles (Fig. 8(b) and 8(c)) were more homogeneous than that of A. However, the height of the nozzle played on the empty space between the overlapped lines. Here, the higher the nozzle, the better the coating.

Surprisingly for us the results show that the thickness and amplitude (or oscillation) of the coating depend on the property of the purchased Pt/C. Because the Pt weight was the same for both catalysts, it is assumed that the properties of the carbon support (e.g. size and porosity) on which the Pt was synthesized play a role in the thickness of the samples. There is a difference of about 3 µm between the samples prepared with the two catalysts. It seems to us that this difference is quite important and can affect water management and gas transport. In general, we (newcomers in coating) pay a lot of attention to the weight of Pt when purchasing Pt/C catalysts but the properties of the carbon support (particle size, micro-porosity, wettability, interaction with the ionomer/solvent, etc.) are equally important. However, it is quite unfortunate that there is not much information on Pt/C (especially concerning unnamed carbon black) when purchasing such catalysts, whereas the price remains expensive regardless carbon support. Ideally, a thorough characterization of the powder should be carried out before processing. It is quite unfortunate that there is not much information on Pt/C when purchasing such catalysts, in particular about the size of the carbon particles.

Regarding the amplitude of the obtained coatings, it seems that this parameter depends on the properties of the Pt/C as well as on the chosen configuration. In the case of the configuration A (Fig. 8(a)), the two catalysts gave two kinds of amplitude although the frequency (period of overlap repetition) was the same. Besides, the amplitude of AA 40 % Pt/C (2021) shown in Fig. 8(a) could not be modeled correctly with the model described in section 2.2.3. The latter could estimate an average thickness, predict the frequency well, but could not accurately estimate the amplitude of the deposited layers. Here, we specify that the reference spectra were obtained by accumulating 4 deposited layers at a same nozzle height and that one spray layer was calculated by dividing the obtained profile by 4. In doing so, we neglected the possible combined effects of overlap, local shadowing and spraying force that are expected to occur during the coating process. Perhaps, for this reason, our model cannot predict well the amplitude of the coating.

When the amplitude was rather negligible as in the case of configuration C (Fig. 8(c)), the fit appeared to match the measurement. For sample B (Fig. 8(b) fit curve in green), we can see that our model gave an average of the measured oscillation, and the fit seemed very smooth compared to the measured profile. In fact, it seems to us that a repetition period can be observed from the measured profile. However, this variation in oscillation cannot be well predicted with our model, perhaps due to a change in the behavior of the reference spectrum ([f(*x*;4,7,1,11,6,1,7µm)] and [f(*x*;4,1,3,11,3,1,1µm)] for nozzle heights of 40 and 60 mm, respectively) or for the reasons cited above regarding amplitude. On the basis of this

observation, it seems to us that a simple model is not enough to perfectly fit the shape of the measured coating. Other, less controllable variables influence the final shape or property of the coating. For example, Deschamps et al. [42] showed that the roughness of the coating layer varies with the carbon samples and the thickness of the coating: the measured roughness of the deposited layer doubled when the thickness layer was doubled for a given carbon sample.

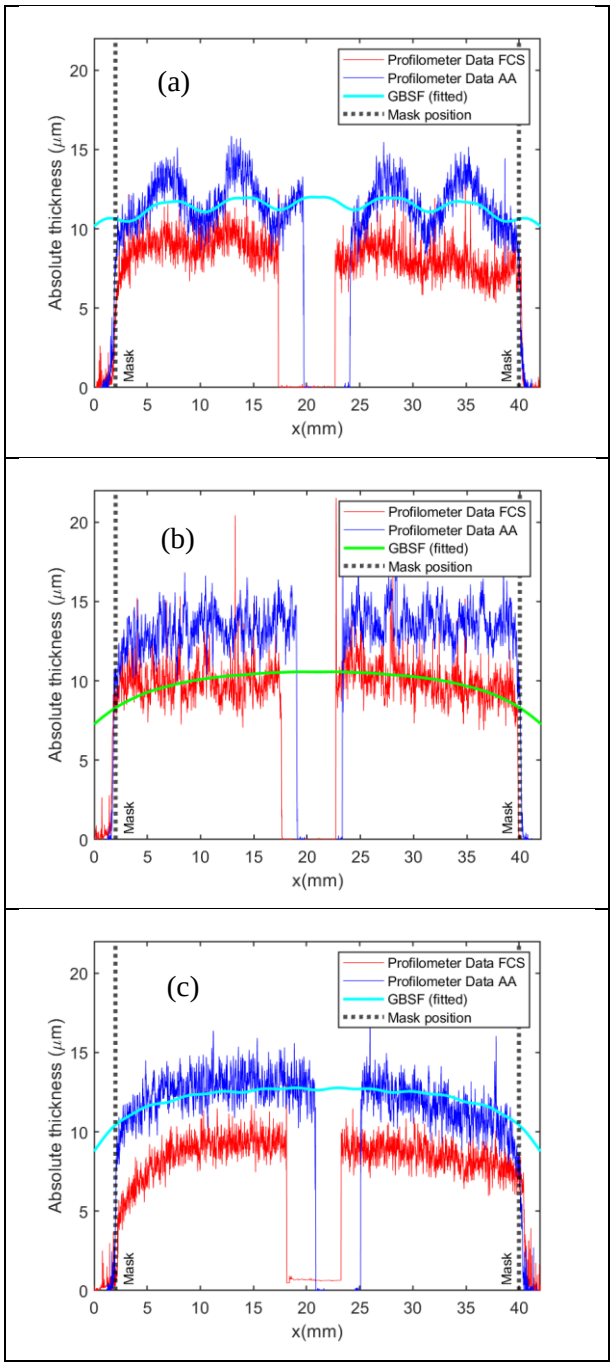

Figure 8. Thickness profiles obtained with the two Pt/C powders (AA40 % Pt/C (2021) and FCS 40 % Pt/C-black (2020) in blue and red, respectively) for the three configurations studied with (a) A – 1 layer of spray pattern repeated 12 times at the nozzle height of 60 mm, (b) B – 2 vertical and 2 horizontal layers of spray pattern repeated 3 times at 40mm and (c) C – 2 vertical and 2 horizontal layers of spray pattern repeated 3 times at 60 mm and MatLAB software fit with GBSF (Generalized Bell-shaped Function).

3.3. Impact on CCMs performance: mask thickness, spray configuration, and Pt/C powder

After correlating the coating parameters with the thickness profile, we investigated the effect of the coating parameters on PEMFC performance. C spray configuration was retained for this section.

3.3.1. Impact of mask thickness

Before studying the impact of the mask on the performance of PEMFC, we checked the coating homogeneity of our lab-made CCMs in terms of the repeatability of the performance. If our coating layers were repeatable, then both sides of our CCM should give the same performance in the fuel cell. In this process, we tested the two configurations shown in Fig. 3. The polarization curves of the two tested configurations are illustrated in Fig. 9(a) and show well the same behavior for both sides of our CCM spray coated with a 1 mm thick PC mask. Furthermore, the two deposited layers have similar electrochemical surface areas, that is, 15.5 and 16.3 $m^2.g_{Pt}$ for sides 1 and 2, respectively, suggesting here that the catalyst deposited on the coating bench was well controlled.

After assuring the quality of our coating in terms of repeatability of performance, the CCMs coated with glass and PC masks were evaluated in a PEMFC bench. Fig. 9(b) compares the polarization curves of samples coated with 10 mm thick glass (red) and 1 mm thick PC (blue) masks. Of course, the more homogeneous coating obtained with the thinner mask gave superior performance. A difference of 0.12 $A.cm^{-2}$ was recorded at 0.6 V between the two curves. This high sensitivity to the shadowing effect is explained by the relative importance of the edges compared to the total surface for this small active area. This effect should be kept in mind because generally, in the laboratory, small active areas are used to characterize new materials that are produced in small quantities.

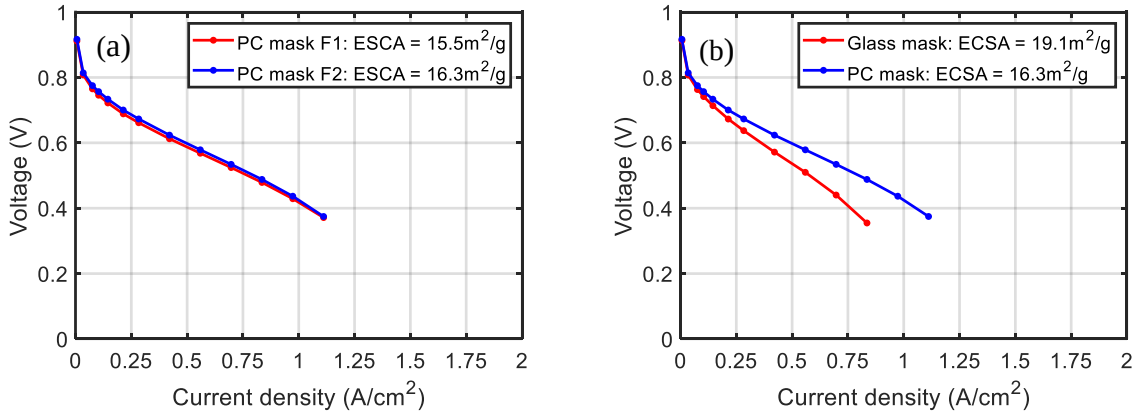

Figure 9. Polarization curves of MEAs with Nafion® 212: (a) reproducibility of MEAs with Nafion 212® sprayed using (a) thin PC masks, and (b) thick glass and thin PC masks,

illustrating the shadowing effect. All results were obtained with Pt/C from Alfa Aesar (AA 40 % Pt/C (2021)) and carried out in H_2 / air at stoichiometry 1.5/5, at 70 °C and 60 % RH for both gases.

3.3.2. Spray configuration patterns

Turning now to the samples prepared with the three pattern configurations (A, B, and C), the polarization curves shown in Fig. 10 indicate that the three spraying configurations give rather similar performance, except in the mass transport region. We can see that the more heterogeneous the coating, the more the mass transport is affected. Additionally, since the 3 samples were obtained after 12 layers of coating for a given ink, the three samples have similar thickness (previous section). As a consequence, the Pt loading (calculated from equation (6)) of the three samples was quite similar (Table 1) and is in good agreement with the literature [29, 39]. Concerning now the ECSA of these samples (Table 1), the two samples prepared with configuration A and C respectively at the same nozzle height, have similar ECSA, 24.7 $m^2.g^{-1}$, and 25.8 $m^2.g^{-1}$ respectively. On the contrary, the sample prepared at a nozzle height of 40 mm is slightly thicker than the other two samples, suggesting here that the nozzle height affects not only the width of the deposited line but also the features of deposited particles after solvent evaporation. The latter may play a role in the roughness of the deposited layer and may explain the difference in the ECSA values. Besides, it is known from the literature data [38, 46] that the height of the nozzle affects the quality of the coating and therefore the fuel cell performance. Indeed, it has been shown that spraying at a low nozzle height can lead to cracks in the coating layer and this can have an impact on the fuel cell performance. However, samples prepared at the same nozzle height and with similar average Pt loading can differ in terms of performance, highlighting here that other phenomena influence mass transport. It can be seen here that it is desirable to produce a catalytic layer that is homogeneous in thickness. From this comparison, we can state that C is the best spray configuration to achieve a homogeneous coating and better fuel cell performance.

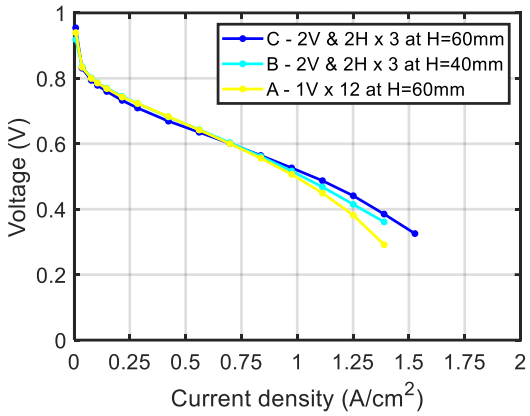

Figure 10. Polarization curves of the CCMs prepared with Pt/C from different suppliers and origins, measured in H_2 / air at stoichiometry 1.5/5, at 70 °C and 60 % RH for both gases.

Table 1. Electrochemical surface area and Pt mass loading of CCMs prepared following 3 different configurations.

Configuration	ECSA ($m^2.g^{-1}$)	Pt mass loading ($mg.cm^{-2}$)
A - 1V x 12 at H=60mm	24.7	0.36
B - 2V & 2H x 3 at H=40mm	31.4	0.37
C - 2V & 2H x 3 at H=60mm	25.8	0.34

3.3.3. Pt/C issues: storage and suppliers

Here, we would like to deal with CCMs prepared with Pt/C powders from different origins using the C spray configuration. We compared the polarization curves of samples prepared with Pt/C powders (40 wt %) from: (i) 2 different suppliers (Alfa Aesar (AA) and Fuel Cell Store (FCS)), (ii) 2 different batches but from the same supplier (AA 2020 and 2021), (iii) at least 2 types of carbon supports (Vulcan XC – 72R and nameless carbon black), and (iv) the same Pt/C but tested at a different time (FCS 40 % Pt/C-Vulcan as-received and FCS 40 % Pt/C-Vulcan 6 months later). Fig. 11 shows the polarization curves of the different CCMs prepared with the different Pt/C powders, but with the same recipe (mentioned in 2.2.1). All studied CCMs have a Pt loading (calculated from equation (6)) rather similar ranged from 0.33 to 0.37 $mg.cm^{-2}$, except for the FCS 40 % Pt/C-Vulcan BS 6 months later and FSC 40 % Pt/C-Black (2020), which are close to 0.4 $mg.cm^{-2}$ (Table 2) All plots with solid lines in Fig. 11 represent samples prepared with catalysts as-received. The single dotted line shows the

behavior of the catalyst FCS 40 % Pt/C-Vulcan opened and reused after 6 months of storage in an ordinary chemical cabinet.

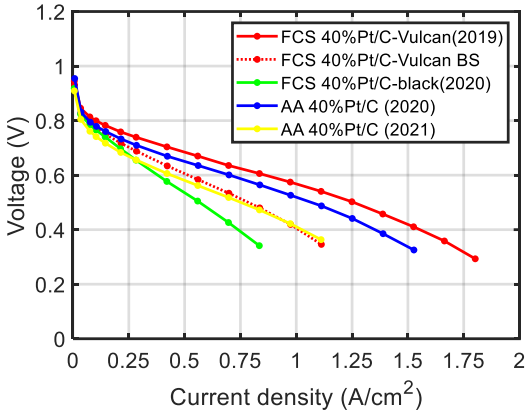

Figure 11. Polarization curves of the CCMs prepared with Pt/C from different suppliers and origins, measured in H_2 / air at stoichiometry 1.5/5, at 70 °C and 60 % RH for both gases (the dashed curve is the sample FCS 40 % Pt/C-Vulcan 6 months later referred as FCS 40 % Pt/C-Vulcan BS).

Among the four Pt/C studied as-received, we can clearly observe that FCS 40 % Pt/C-Vulcan (2019) from Fuel Cell Store (red solid line) gave the best polarization curve for a given ink recipe. The worst performance was given by the FCS 40 % Pt/C-black, whereas the coating thickness was thinner than that prepared with AA 40 % Pt/C (2021), despite comparatively higher Pt loading (Table 2). This comparison reveals that: (i) each Pt/C powder is unique, i.e. the carbon-support can be different in size and porosity and it could be the same for Pt crystallites and impurities, and (ii) the change of Pt/C suppliers, batches, and carbon supports can randomly affect the PEMFC performance. Therefore, point (i) above can explain the difference in ECSA showed in the Table 2 for different origins and batches of Pt/C.

Table 2. Electrochemical surface area and Pt mass loading of CCMs prepared with Pt/C from different suppliers and origins.

Configuration	ECSA	Pt mass loading
	($m^2.g^{-1}$)	($mg.cm^{-2}$)
FCS 40 % Pt/C-Vulcan(2019)	36.5	0.34
FCS 40 % Pt/C-Vulcan BS	23.8	0.39
FCS 40 % Pt/C-black (2020)	16.3	0.42

AA 40 % Pt/C (2020)	27.9	0.37
AA 40 % Pt/C (2021)	15.1	0.33

Now comparing the sample prepared with as-received FCS 40 % Pt/C-Vulcan (2019) and the one prepared 6 months later with the same catalyst, the results point out that the performance of the catalyst decreased with storage time (0.85 vs. 0.50 $A.cm^{-2}$ at 0.6V, respectively). This feature was rather unexpected since Pt metal is known to be stable at room temperature. In fact, bulk Pt or Pt film is stable under ambient conditions, but not nano-sized Pt particles or clusters [50, 51]. Indeed, Banarjee et al. [52] studied by XPS the oxidation of Pt particles of 1-4 nm on different carbon supports. The characterized samples were exposed to ambient air for 8 h to 1 week. Their results clearly showed that small Pt sizes, less than 1.4 nm, were mainly oxidized (80 %) and Pt particles larger than 1.4 nm were less oxidized (about 30 %). The latter represents the shell of Pt particles but the core remains Pt(0). From the literature results, it seems that keeping Pt/C away from oxygen or air is paramount to avoid its oxidation and maintains its performance in the PEMFC.

Thus, the results in PEMFC can vary depending on the size distribution of Pt and also on the amount of Pt(II) and Pt(IV), which do not participate in the catalyst activity. Concerning the sample prepared with FCS 40 % Pt/C-Vulcan (2019) 6 months later (the red dashed curve in Fig. 11), it is possible according to literature that the Pt oxidation phenomenon is responsible for the decrease of the performance measured in the PEMFC. This hypothesis will be confirmed or refute by our forthcoming work.

4. Conclusion

Mastering the coating bench for PEMFC catalyst layers can be time-consuming but is necessary to obtain repeatable coatings. In this sense, the experimental part of this paper was detailed in order to help beginners in spray-coating. The objective of this research was to identify some key parameters to improve the coating and its impact on fuel cell performance via modeling and measurements of the coating thickness as well as via polarization curves in the PEMFC bench. Through our work, it seems to us that the mask thickness, the spray configuration (pattern and height of nozzle) and the properties of catalyst powders affect a lot the homogeneity and the thickness of the coating layer and also its performance in PEMFC. Moreover, the results of this study lead to the following conclusions:

- Pt/C powders from different suppliers or different batches from same supplier are not equivalent, and this plays a role in the PEMFC performance for a given recipe and coating mode.
- CCMs prepared with stored Pt/C powder give lower performance in PEMFC compared to CCMs prepared with as-received Pt/C powder.
- The thickness of the coating and its profile depend on the origin of Pt/C powder. And the configuration of its coating affects the PEMFC performance. It is desirable to manufacture catalyst layers of homogeneous thickness. Prior to coating, a MatLAB simulation can help optimize the configuration
- The thickness of the mask also affects the homogeneity of the coating. The thinner the mask, the more homogeneous the coating. This effect is not negligible for MEAs with a small active surface area.

References

[1] S. Shahgaldi, I. Alaefour, and X. Li, "Impact of manufacturing processes on proton exchange membrane fuel cell performance," *Appl. Energy*, vol. 225, no. May, pp. 1022–1032, 2018, doi: 10.1016/j.apenergy.2018.05.086.

[2] C. Coutanceau, M. Chatenet, D. Jones, and G. Maranzana, "12 Materials for proton-exchange fuel cell for mobility and stationary applications," in *Utilization of Hydrogen for Sustainable Energy and Fuels*, De Gruyter, 2021, pp. 399–432. doi: 10.1515/9783110596274-020.

[3] M. Chen, C. Zhao, F. Sun, J. Fan, H. Li, and H. Wang, "Research progress of catalyst layer and interlayer interface structures in membrane electrode assembly (MEA) for proton exchange membrane fuel cell (PEMFC) system," *eTransportation*, vol. 5, p. 100075, 2020, doi: 10.1016/j.etran.2020.100075.

[4] A. Kusoglu and A. Z. Weber, "New Insights into Perfluorinated Sulfonic-Acid Ionomers," *Chem. Rev.*, vol. 117, no. 3, pp. 987–1104, 2017, doi: 10.1021/acs.chemrev.6b00159.

[5] K. A. Mauritz and R. B. Moore, "State of understanding of Nafion," *Chem. Rev.*, vol. 104, no. 10, pp. 4535–4585, 2004, doi: 10.1021/cr0207123.

[6] F. D. Coms, H. Liu, and J. E. Owejan, "Mitigation of Perfluorosulfonic Acid Membrane Chemical Degradation Using Cerium and Manganese Ions," *ECS Trans.*, vol. 16, no. 2, pp. 1735–1747, Dec. 2019, doi: 10.1149/1.2982015.

[7] M. Breitwieser, M. Klingele, B. Britton, S. Holdcroft, R. Zengerle, and S. Thiele, "Improved Pt-utilization efficiency of low Pt-loading PEM fuel cell electrodes using direct membrane deposition," *Electrochem. commun.*, vol. 60, pp. 168–171, 2015, doi: 10.1016/j.elecom.2015.09.006.

[8] S. Vierrath, M. Breitwieser, M. Klingele, B. Britton, S. Holdcroft, R. Zengerle, and S. Thiele, "The reasons for the high power density of fuel cells fabricated with directly deposited membranes," *J. Power Sources*, vol. 326, pp. 170–175, 2016, doi: 10.1016/j.jpowsour.2016.06.132.

[9] S. Park, J. W. Lee, and B. N. Popov, "A review of gas diffusion layer in PEM fuel cells: Materials and designs," *Int. J. Hydrogen Energy*, vol. 37, no. 7, pp. 5850–5865, 2012, doi: 10.1016/j.ijhydene.2011.12.148.

[10] E. H. Majlan, D. Rohendi, W. R. W. Daud, T. Husaini, and M. A. Haque, "Electrode for proton exchange membrane fuel cells: A review," *Renew. Sustain. Energy Rev.*, vol. 89,

no. April, pp. 117–134, 2018, doi: 10.1016/j.rser.2018.03.007.

[11] A. Ozden, S. Shahgaldi, X. Li, and F. Hamdullahpur, “A review of gas diffusion layers for proton exchange membrane fuel cells—With a focus on characteristics, characterization techniques, materials and designs,” *Prog. Energy Combust. Sci.*, vol. 74, pp. 50–102, 2019, doi: 10.1016/j.pecs.2019.05.002.

[12] Y. Wang, H. Yuan, A. Martinez, P. Hong, H. Xu, and F. R. Bockmiller, “Polymer electrolyte membrane fuel cell and hydrogen station networks for automobiles: Status, technology, and perspectives,” *Adv. Appl. Energy*, vol. 2, p. 100011, May 2021, doi: 10.1016/j.adapen.2021.100011.

[13] G. Frenette and D. Forthoffer, “Economic & commercial viability of hydrogen fuel cell vehicles from an automotive manufacturer perspective,” *Int. J. Hydrogen Energy*, vol. 34, no. 9, pp. 3578–3588, May 2009, doi: 10.1016/j.ijhydene.2009.02.072.

[14] L. Duclos, M. Lupsea, G. Mandil, L. Svecova, P.-X. Thivel, and V. Laforest, “Environmental assessment of proton exchange membrane fuel cell platinum catalyst recycling,” *J. Clean. Prod.*, vol. 142, pp. 2618–2628, Jan. 2017, doi: 10.1016/j.jclepro.2016.10.197.

[15] A. E. Hughes, N. Haque, S. A. Northey, and S. Giddey, “Platinum Group Metals: A Review of Resources, Production and Usage with a Focus on Catalysts,” *Resources*, vol. 10, no. 9, p. 93, Sep. 2021, doi: 10.3390/resources10090093.

[16] J. Stacy, Y. N. Regmi, B. Leonard, and M. Fan, “The recent progress and future of oxygen reduction reaction catalysis: A review,” *Renew. Sustain. Energy Rev.*, vol. 69, pp. 401–414, Mar. 2017, doi: 10.1016/j.rser.2016.09.135.

[17] L. Bouleau, S. Pérez-Rodríguez, J. Quílez-Bermejo, M. T. Izquierdo, F. Xu, V. Fierro, and A. Celzard, “Best practices for ORR performance evaluation of metal-free porous carbon electrocatalysts,” *Carbon N. Y.*, vol. 189, pp. 349–361, Apr. 2022, doi: 10.1016/j.carbon.2021.12.078.

[18] T. Poux, F. S. Napolskiy, T. Dintzer, G. Kéranguéven, S. Y. Istomin, G. A. Tsirlina, E. V. Antipov, and E. R. Savinova, “Dual role of carbon in the catalytic layers of perovskite/carbon composites for the electrocatalytic oxygen reduction reaction,” *Catal. Today*, vol. 189, no. 1, pp. 83–92, Jul. 2012, doi: 10.1016/j.cattod.2012.04.046.

[19] S. Martens, L. Asen, G. Ercolano, F. Dionigi, C. Zalitis, A. Hawkins, A. Martinez Bonastre, L. Seidl, A. C. Knoll, J. Sharman, P. Strasser, D. Jones, and O. Schneider, “A comparison of rotating disc electrode, floating electrode technique and membrane electrode assembly measurements for catalyst testing,” *J. Power Sources*, vol. 392, no.

April, pp. 274–284, 2018, doi: 10.1016/j.jpowsour.2018.04.084.

[20] C. M. Zalitis, D. Kramer, and A. R. Kucernak, “Electrocatalytic performance of fuel cell reactions at low catalyst loading and high mass transport,” *Phys. Chem. Chem. Phys.*, vol. 15, no. 12, pp. 4329–4340, 2013, doi: 10.1039/c3cp44431g.

[21] Indriyati, Y. Irmawati, and B. Prihandoko, “Preparation of catalyst coated membrane by modified decal transfer method for proton exchange membrane fuel cell,” *IOP Conf. Ser. Mater. Sci. Eng.*, vol. 223, no. 1, 2017, doi: 10.1088/1757-899X/223/1/012037.

[22] S. Shahgaldi, I. Alaefour, G. Unsworth, and X. Li, “Development of a low temperature decal transfer method for the fabrication of proton exchange membrane fuel cells,” 2017, doi: 10.1016/j.ijhydene.2017.02.127.

[23] H. J. Cho, H. Jang, S. Lim, E. Cho, T.-H. Lim, I.-H. Oh, H.-J. Kim, and J. H. Jang, “Development of a novel decal transfer process for fabrication of high-performance and reliable membrane electrode assemblies for PEMFCs,” 2011, doi: 10.1016/j.ijhydene.2011.06.113.

[24] W. Wang, S. Chen, J. Li, and W. Wang, “Fabrication of catalyst coated membrane with screen printing method in a proton exchange membrane fuel cell,” 2015, doi: 10.1016/j.ijhydene.2015.02.027.

[25] A. Bayrakçeken, S. Erkan, L. Türker, and I. Eroğlu, “Effects of membrane electrode assembly components on proton exchange membrane fuel cell performance,” *Int. J. Hydrogen Energy*, vol. 33, no. 1, pp. 165–170, 2008, doi: 10.1016/j.ijhydene.2007.08.021.

[26] B. H. Lim, E. H. Majlan, A. Tajuddin, T. Husaini, W. R. Wan Daud, N. A. Mohd Radzuan, and M. A. Haque, “Comparison of catalyst-coated membranes and catalyst-coated substrate for PEMFC membrane electrode assembly: A review,” *Chinese J. Chem. Eng.*, vol. 33, pp. 1–16, 2021, doi: 10.1016/j.cjche.2020.07.044.

[27] S. Shukla, K. Domican, K. Karan, S. Bhattacharjee, and M. Secanell, “Analysis of low platinum loading thin polymer electrolyte fuel cell electrodes prepared by inkjet printing,” *Electrochim. Acta*, vol. 156, pp. 289–300, 2014, doi: 10.1016/j.electacta.2015.01.028.

[28] B. Millington, V. Whipple, and B. G. Pollet, “A novel method for preparing proton exchange membrane fuel cell electrodes by the ultrasonic-spray technique,” *J. Power Sources*, vol. 196, no. 20, pp. 8500–8508, 2011, doi: 10.1016/j.jpowsour.2011.06.024.

[29] T. H. Huang, H. L. Shen, T. C. Jao, F. B. Weng, and A. Su, “Ultra-low Pt loading for proton exchange membrane fuel cells by catalyst coating technique with ultrasonic spray

coating machine," *Int. J. Hydrogen Energy*, vol. 37, no. 18, pp. 13872–13879, 2012, doi: 10.1016/j.ijhydene.2012.04.108.

[30] I. Fouzaï, S. Gentil, V. C. Bassetto, W. O. Silva, R. Maher, and H. H. Girault, "Catalytic layer-membrane electrode assembly methods for optimum triple phase boundaries and fuel cell performances," *J. Mater. Chem. A*, vol. 9, no. 18, pp. 11096–11123, 2021, doi: 10.1039/d0ta07470e.

[31] A. M. Chaparro, M. A. Folgado, P. Ferreira-Aparicio, A. J. Martín, I. Alonso-Álvarez, and L. Daza, "Properties of Catalyst Layers for PEMFC Electrodes Prepared by Electrospray Deposition," *J. Electrochem. Soc.*, vol. 157, no. 7, p. B993, 2010, doi: 10.1149/1.3425740.

[32] S. A. Mauger, J. R. Pfeilsticker, M. Wang, S. Medina, A. C. Yang-Neyerlin, K. C. Neyerlin, C. Stetson, S. Pylypenko, and M. Ulsh, "Fabrication of high-performance gas-diffusion-electrode based membrane-electrode assemblies," *J. Power Sources*, vol. 450, no. January, p. 227581, 2020, doi: 10.1016/j.jpowsour.2019.227581.

[33] R. Benítez, J. Soler, and L. Daza, "Novel method for preparation of PEMFC electrodes by the electrospray technique," *J. Power Sources*, vol. 151, no. 1–2, pp. 108–113, 2005, doi: 10.1016/j.jpowsour.2005.02.047.

[34] M. Stähler, A. Stähler, F. Scheepers, M. Carmo, and D. Stolten, "A completely slot die coated membrane electrode assembly," *Int. J. Hydrogen Energy*, vol. 44, no. 14, pp. 7053–7058, 2019, doi: 10.1016/j.ijhydene.2019.02.016.

[35] N. Kapur, "A parametric study of direct gravure coating," *Chem. Eng. Sci.*, vol. 58, no. 13, pp. 2875–2882, 2003, doi: 10.1016/S0009-2509(03)00136-2.

[36] J. Park, Z. Kang, G. Bender, M. Ulsh, and S. A. Mauger, "Roll-to-roll production of catalyst coated membranes for low-temperature electrolyzers," *J. Power Sources*, vol. 479, no. August, p. 228819, 2020, doi: 10.1016/j.jpowsour.2020.228819.

[37] E. B. Creel, K. Tjiptowidjojo, J. Alex Lee, K. M. Livingston, P. Randall Schunk, N. S. Bell, A. Serov, and D. L. Wood, "Slot-die-coating operability windows for polymer electrolyte membrane fuel cell cathode catalyst layers," *J. Colloid Interface Sci.*, vol. 610, pp. 474–485, 2022, doi: 10.1016/j.jcis.2021.11.047.

[38] S. Martin, J. O. Jensen, Q. Li, P. L. Garcia-Ybarra, and J. L. Castillo, "Feasibility of ultra-low Pt loading electrodes for high temperature proton exchange membrane fuel cells based in phosphoric acid-doped membrane," *Int. J. Hydrogen Energy*, vol. 44, no. 52, pp. 28273–28282, 2019, doi: 10.1016/j.ijhydene.2019.09.073.

[39] M. B. Sassin, Y. Garsany, R. W. Atkinson, R. M. E. Hjelm, and K. E. Swider-Lyons,

"Understanding the interplay between cathode catalyst layer porosity and thickness on transport limitations en route to high-performance PEMFCs," *Int. J. Hydrogen Energy*, vol. 44, no. 31, pp. 16944–16955, Jun. 2019, doi: 10.1016/j.ijhydene.2019.04.194.

[40] B. G. Pollet, "The Use of Power Ultrasound for the Production of PEMFC and PEMWE Catalysts and Low-Pt Loading and High-Performing Electrodes," *Catal. 2019, Vol. 9, Page 246*, vol. 9, no. 3, p. 246, Mar. 2019, doi: 10.3390/CATAL9030246.

[41] T.-C. Jao, G.-B. Jung, H.-L. Shen, C.-C. Yeh, Y.-J. Su, T.-C. Jao, G.-B. Jung, H.-L. Shen, C.-C. Yeh, and Y.-J. Su, "Ultrasonic Spray Coating for Proton Exchange Membrane Fuel Cell," *Open J. Acoust.*, vol. 3, no. 3, pp. 33–37, Sep. 2013, doi: 10.4236/OJA.2013.33A006.

[42] F. L. Deschamps, J. G. Mahy, A. F. Léonard, S. D. Lambert, A. Dewandre, B. Scheid, and N. Job, "A practical method to characterize proton exchange membrane fuel cell catalyst layer topography: Application to two coating techniques and two carbon supports," *Thin Solid Films*, vol. 695, no. December 2019, p. 137751, Feb. 2020, doi: 10.1016/j.tsf.2019.137751.

[43] S. Litster and G. McLean, "PEM fuel cell electrodes," *J. Power Sources*, vol. 130, no. 1–2, pp. 61–76, 2004, doi: 10.1016/j.jpowsour.2003.12.055.

[44] G. Y. Chen, C. Wang, Y. J. Lei, J. Zhang, Z. Mao, Z. Q. Mao, J. W. Guo, J. Li, and M. Ouyang, "Gradient design of Pt/C ratio and Nafion content in cathode catalyst layer of PEMFCs," *Int. J. Hydrogen Energy*, vol. 42, no. 50, pp. 29960–29965, 2017, doi: 10.1016/j.ijhydene.2017.06.229.

[45] H. Yu, J. M. Roller, W. E. Mustain, and R. Maric, "Influence of the ionomer/carbon ratio for low-Pt loading catalyst layer prepared by reactive spray deposition technology," *J. Power Sources*, vol. 283, pp. 84–94, 2015, doi: 10.1016/j.jpowsour.2015.02.101.

[46] M. B. Sassin, Y. Garsany, B. D. Gould, and K. E. Swider-Lyons, "Fabrication Method for Laboratory-Scale High-Performance Membrane Electrode Assemblies for Fuel Cells," *Anal. Chem.*, vol. 89, no. 1, pp. 511–518, 2017, doi: 10.1021/acs.analchem.6b03005.

[47] N. Talpur, M. N. M. Salleh, and K. Hussain, "An investigation of membership functions on performance of ANFIS for solving classification problems," *IOP Conf. Ser. Mater. Sci. Eng.*, vol. 226, no. 1, 2017, doi: 10.1088/1757-899X/226/1/012103.

[48] J. Dillet, D. Spernjak, A. Lamibrac, G. Maranzana, R. Mukundan, J. Fairweather, S. Didierjean, R. L. Borup, and O. Lottin, "Impact of flow rates and electrode specifications on degradations during repeated startups and shutdowns in polymer-electrolyte

membrane fuel cells," *J. Power Sources*, vol. 250, pp. 68–79, 2014, doi: 10.1016/j.jpowsour.2013.10.141.

[49] A. Lamibrac, "Study of the degradations induced by start-up/shut-down operations in PEMFC," *Lemta*, vol. Doctorate, p. 240, 2013.

[50] R. Banerjee, Q. Liu, J. M. M. Tengco, and J. R. Regalbuto, "Detection of Ambient Oxidation of Ultrasmall Supported Platinum Nanoparticles with Benchtop Powder X-Ray Diffraction," *Catal. Lett. 2017 1477*, vol. 147, no. 7, pp. 1754–1764, May 2017, doi: 10.1007/S10562-017-2060-2.

[51] J. R. Gallagher, T. Li, H. Zhao, J. Liu, Y. Lei, X. Zhang, Y. Ren, J. W. Elam, R. J. Meyer, R. E. Winans, and J. T. Miller, "In situ diffraction of highly dispersed supported platinum nanoparticles †," *Cite this Catal. Sci. Technol*, vol. 4, p. 3053, 2014, doi: 10.1039/c4cy00414k.

[52] R. Banerjee, D. A. Chen, S. Karakalos, M. L. C. Piedboeuf, N. Job, and J. R. Regalbuto, "Ambient Oxidation of Ultrasmall Platinum Nanoparticles on Microporous Carbon Catalyst Supports," *ACS Appl. Nano Mater.*, vol. 1, no. 10, pp. 5876–5884, Oct. 2018, doi: 10.1021/acsanm.8b01548.